Photocatalytic Activity of Boron-Modified Titania under UV and Visible-Light Illumination

Václav Štengl, Vendula Houšková,* Snejana Bakardjieva, and Nataliya Murafa

Institute of Inorganic Chemistry, Academy of Science of the Czech Republic, v.v.i.,
250 68 Husinec-Rez, Czech Republic

ABSTRACT Nanosized boron(III) oxide-doped titania was prepared by homogeneous hydrolysis of titanium oxo-sulfate with urea in aqueous solutions in the presence of amorphous boron. The prepared samples were annealing at 700 °C. The structure of as-prepared samples was characterized by X-ray powder diffraction (XRD) and selected area electron diffraction (SAED) and surface area (BET) and porosity determination (BJH). The morphology and microstructure characteristics were obtained by scanning electron microscopy (SEM) and high-resolution electron microscopy (HRTEM). The method of UV/vis diffuse reflectance spectroscopy was employed to estimate band gap energies of the boron-doped titania. The photoactivity of the prepared samples was assessed by the photocatalytic decomposition of Orange II dye in an aqueous slurry during irradiation at 365 and 400 nm wavelength. The prepared titania samples doped with boron(III) oxide showed better photocatalytic activity in comparison with the reference TiO_2 sample. These photocatalysts showed better photocatalytic performance under visible-light irradiation.

KEYWORDS: anatase • boron • doping • homogeneous hydrolysis • photocatalytic activity

1. INTRODUCTION

To improve the photocatalytic performance of titania under visible light, a boron and nitrogen codoped titania photocatalyst was prepared from boric acid (H_3BO_3), ammonium fluoride (NH_4F) and tetrabutyl titanate ($Ti(O-C_4H_9)_4$) (1). A series of nanosized boron-doped and boron−iron codoped anatase TiO_2 represented as B_x,Fe_y-TiO_2 ($x = 1, 3, 5$; $y = 0, 0.5, 1, 3, 5$ in wt %) were synthesized by a modified sol−gel method, and characterized by various spectroscopic and analytical techniques. The presence of boron and/or iron causes a red shift in the absorption band of TiO_2 (2). A boron/ferrum/cerium/titania photocatalyst with visible-light-induced performance was prepared by the conventional sol−gel method, in which tetrabutyl titanate ($Ti(O\text{-}nC_4H_9)_4$) was used as the precursor and boric acid (H_3BO_3), ferric nitrate enneahydrate ($Fe(NO_3)_3 \cdot 9H_2O$), and cerium nitrate hexahydrate ($Ce(NO_3)_3 \cdot 6H_2O$) were the sources of boron, ferrum, and cerium, respectively (3). The boron, nickel, and cerium ternary codoped photocatalyst exhibiting high photoactivity in the visible region was prepared by the sol−gel method (4). Authors testified that boron doping led to the response to visible light and that nickel and cerium doping prohibited the recombination of the photogenerated electron−hole pairs, improving the photocatalytic performance. The results showed that the synergistic effects of boron, nickel, and cerium codoping played an important role in raising photoactivity. The work (5) was dedicated to the tailored synthesis of TiO_2 nanopowders doped with boron, nitrogen for the photocatalytic degradation of organic dyes. The Pd−B/TiO_2 amorphous alloy catalyst was prepared by the liquid-phase chemical reduction with KBH_4 aqueous solution (6). New boron-doped titanium dioxide catalysts were prepared using the sol−gel and mortar and pestle pulverization and mixing preparation procedures (7). Boron and cerium codoped TiO_2 photocatalysts were synthesized using a modified sol−gel method. When boron and cerium were doped, the UV−vis adsorption band wavelength showed an obvious shift toward the visible range (≤526 nm) (8). In the study (9), chemical vapor deposition (CVD) was applied to dope boron into TiO_2 nanotubes, anodized Ti in $C_2H_2O_4 \cdot 2H_2O$+NH_4F electrolyte, with the goal of improving the photocatalytic activity under visible light. The boron-doped TiO_2 nanotube arrays were fabricated by potentiostatic anodization of titanium in an aqueous electrolyte containing fluoride ion and sodium fluoroborate ($NaBF_4$). The highly ordered nanotube arrays with an inner pore diameter of approximately 80 nm and a length of 1.4 μm are obtained (10). The sol−gel route was employed to prepare a titania/silica photocatalyst codoped with boron and ferrum. The synergistic effects of codoping and intimate interaction between titania and silica were responsible for the increase of photoactivity (11). B-TiO_2 photocatalysts were prepared by surface impregnation procedure using boric acid triethyl ester (BATE) as a boron precursor (12). The effect of boron content, calcination temperature, and titanium dioxide source used during preparation procedure (13) on photoactivity was investigated. TiO_2 photocatalysts modified with boron oxides decomposed water stoichiometrically in aqueous suspension systems and photocatalytic activities

* Corresponding author. E-mail: houskova@iic.cas.cz. Tel.: 420 2 6617 3193. Fax: 420 2 2094 1502.
Received for review November 4, 2009 and accepted January 25, 2010
DOI: 10.1021/am9007598

Table 1. Microstructural Characteristics of Titania Samples Heated at 700°C

sample	B loading (g)	anatase by XRD (%)	rutile by XRD (%)	sassolite by XRD (%)	anatase cryst. size (nm)	surface area (BET) (m^2 g^{-1})	pore volume (cc g^{-1})
TiB1_700	0.12	100			60.7	27.4	0.115
TiB2_700	0.25	100			63.7	42.1	0.205
TiB3_700	0.50	100			92.1	15.6	0.661
TiB4_700	0.75	96.5	0.5	3.0	70.5	17.7	0.135
TiB5_700	1.00	93.5	2.9	3.6	97.2	19.3	0.213
TiB6_700	3.00	87.2	5.9	6.9	61.3	5.3	0.086

were strongly dependent on the crystal phase of the titanium oxide in the Pt-loaded B/TiO_2 photocatalyst. Titanium tetra-*n*-butyl oxide (TTB) were used as TiO_2 and boron precursor, the TTB was added dropwise to the H_2O−H_3BO_3 mixed solution under vigorous stirring (14). Boron and vanadium doped TiO_2 photocatalysts were synthesized using modified sol−gel method from titanium(IV) butoxide and boric acid (15).

The aim of the present work was to synthesize B-doped nanoparticles with variable B/Ti ratio and appropriate microstructure characteristics, allowing its application as a photocatalyst in an aqueous solution. Homogeneous hydrolysis of titanium oxo-sulfate with urea in aqueous solution in the presence of amorphous boron has been chosen as a way of synthesis. The obtained precursors were heated at 700 °C. The attention has been paid not only to ratio B/TiO_2 but also to crystal structure, BET surface area, particle size, porosity and the effect of the individual anatase and rutile doped nanocrystals on the photoactivity. The photocatalytic activity was studied under UV and visible light by measuring of Orange II disappearance. Pure undoped TiO_2 sample was used as a comparing standard.

2. EXPERIMENTAL SECTION

2.1. Preparation of Titania Samples Doped with Boron. All chemical reagents used in the presented experiments were obtained from commercial sources and used without further purification. $TiOSO_4$, amorphous boron, and urea were supplied by Fluka, Munich, Germany. The boron-doped titania was prepared by homogeneous hydrolysis of $TiOSO_4$ aqueous solutions using urea as the precipitation agent. In a typical process, 100 g of $TiOSO_4$ was dissolved in 100 mL of hot distilled water acidified with 98% H_2SO_4. The pellucid liquid was diluted into 4 L of distilled water. A defined amount of amorphous boron (see Table 1) and 300 g of urea were added. The mixture was heated to 100 °C under stirring and kept at this temperature for 9 h until pH 7.5 was reached and ammonia escaped from the solution. The formed precipitates were washed by distilled water with decantation, filtered out and dried at temperature of 105 °C in a dry oven. Six new samples denoted as TiB_1 to TiB_6, respectively, were prepared. The reference sample, pure TiO_2, prepared without boron as dopant was denoted as TiB_0. The prepared samples were heated at 700 °C under a dynamic vacuum in the quartz tube for 1 h by using a furnace controlled by the PID controller. The temperature increase rate was 1 °C min^{-1}. After the heat treatment, the sample was allowed to cool at room temperature.

2.2. Characterization Methods. X-ray diffraction (XRD) patterns were obtained by Siemens D5005 instrument using Cu-Ká radiation (40 kV, 30 mA) and a diffracted beam monochromator. Qualitative analysis was performed with the DiffracPlus Eva Application (Bruker AXS) using the JCPDS PDF-2 database (16). For quantitative phase analysis, mean coherence length analysis, and structural refinement, Rietveld analysis with DiffracPlus Topas (Bruker ASX) and structural models from ICSD database were used (17).

Surface areas of the samples outgassed for 60 min at 150 °C were determined from nitrogen adsorption−desorption isotherms at liquid nitrogen temperature using a Coulter SA3100 instrument with outgas 15 min at 120 °C.. The Brunauer−Emmett−Teller (BET) method was used for surface area calculation (18), the pore size distribution (pore diameter and pore volume of samples) was determined by the Barrett−Joyner−Halenda (BJH) method (19).

Scanning electron microscopy (SEM) studies were performed using a Philips XL30 CP microscope equipped with energy-dispersive X-ray (EDX), Robinson, secondary electron (SE), and backscattered electron (BSE) detectors.

High-resolution transmission electron microscopy (HRTEM) was done with transmission electron microscope JEOL JEM 3010 at 300 kV (LaB6 cathode) giving a point resolution of 0.17 nm. A copper grid coated with a holey carbon support film was used to prepare samples for TEM observation. The powdered sample was dispersed in ethanol and the suspension was treated in an ultrasonic bath for 10 min.

DTA-TG measurements were carried out using a simultaneous Netzsch Instrument STA 409 coupled to Quadrupol Mass Spectrometer Balzers QMS-420 under dynamic conditions in the helium (flow rate 40 mL min^{-1}). The samples were heated at the rate of 10 °C min^{-1}.

Diffuse reflectance UV/vis spectra for the evaluation of photophysical properties were recorded in the diffuse reflectance mode (R) and transformed to absorption spectra through the Kubelka−Munk function (20). A Perkin-Elmer Lambda 35 spectrometer equipped with a Labsphere RSA-PE-20 integration sphere with $BaSO_4$ as a standard was used. The band gap was obtained from a plot of the modified Kubelka−Munk function versus the energy of exciting light by converting the scanning wavelength (λ) into photon energies (E_{bg}).

Photocatalytic activity of samples was assessed from the kinetics of the photocatalytic degradation of 0.02 M Orange II dye (sodium salt 4-[(2-hydroxy-1-naphtenyl)azo]-benzenesulfonic acid) in aqueous slurries. Kinetics of the photocatalytic degradation of aqueous Orange II dye solution was measured by using a self-constructed photoreactor (21, 22). The photoreactor consists of a stainless steel cover and quartz tube with fluorescent lamp Narva with power 13W. Black light (365 nm) for UV, warmwhite and Bio light (upon 400 nm), respectively, for visible light irradiation were used. Orange II dye solution was circulated by means of membrane pump through flow cuvette. The concentration of Orange II dye was determined by measuring absorbance at 480 nm with VIS spectrophotometer ColorQuestXE.

3. RESULTS AND DISCUSSION

3.1. X-ray Diffraction (XRD). The powder XRD patterns of B doped titania samples prepared by homogeneous hydrolysis and annealed at 700 °C are presented in Figure 1.

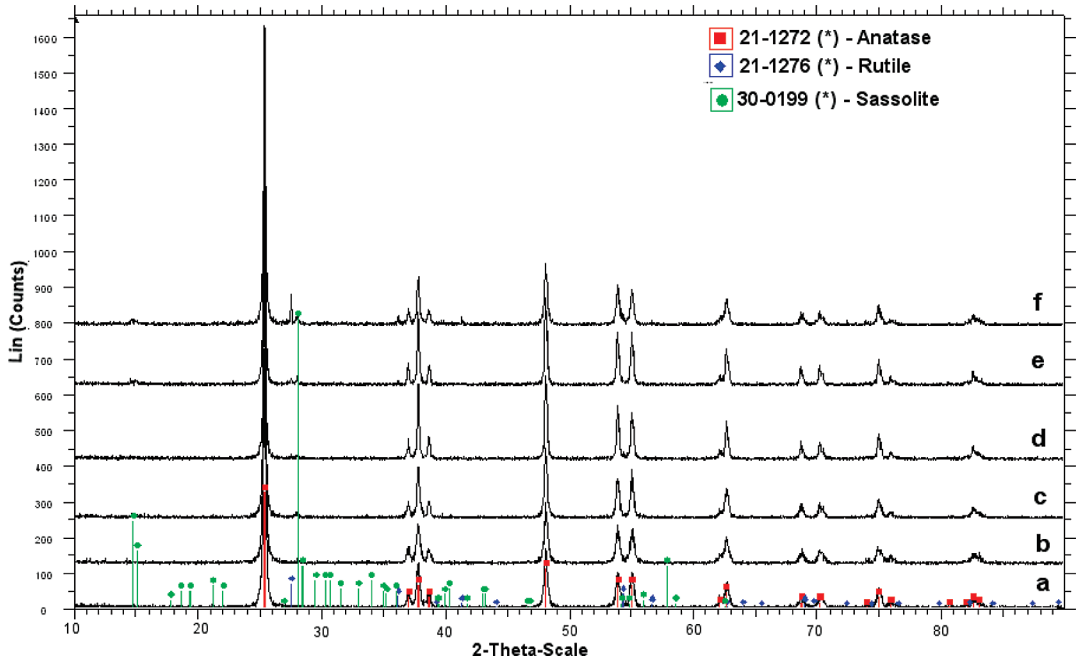

FIGURE 1. XRD pattern of the sample (a) TiB1_700, (b) TiB2_700, (c) TiB3_700, (d) TiB4_700, (e) TiB5_700, (f) TiB6_700. R = TiO_2, rutile, ICDD PDF 21−1276; S= H_3BO_3, sassolite, ICDD PDF 30−0199.

Polycrystalline anatase (ICDD PDF 21−1272) was identified in all samples. Crystallite size and unit-cell parameters of the components were calculated by the Rietveld method and the results are given in Table 1. In samples TiB_1 to TiB_3 neither B-containing phases nor changes of unit-cell of TiO_2 were detected. Considering that the radius of B^{3+} (0.023 nm) is much smaller than that of Ti^{4+} (0.068 nm), it would be difficult for B^{3+} to replace the Ti^{4+} site (14). Thus, it is assumed that boron occupies the interstitials between the TiO_2 crystallites; however, the B amount falls below the responsiveness of the powder X-ray diffraction method and could not be detected. In the samples doped with higher amount of B (TiB_4, TiB_5 and TiB_6), rutile (ICDD PDF 21−1276) and sassolite (H_3BO_3, ICDD PDF 30−0199) were presented. Occurrence of rutile phase in the samples annealed at 700 °C increases with increasing B doping (see Table 1). These results suggest that the temperature of the anatase-rutile transition is dependent on the B content (boron decreases the transition temperature).

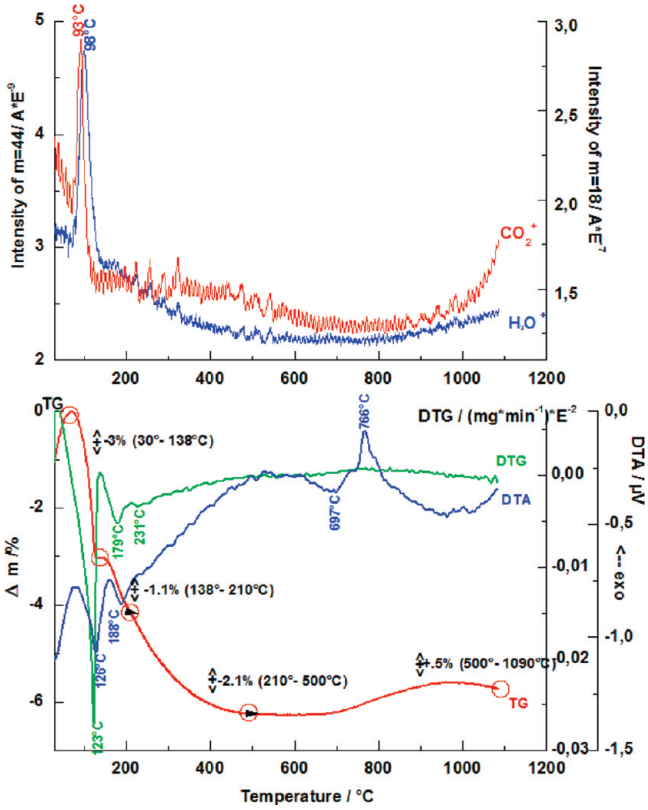

FIGURE 2. DTA-TG curves for the sample TiB_5.

3.2. Thermal Analysis of the Samples.

Figure 2 shows a curve of thermal analysis of the sample TiB_5. DTA and TG curve shows that at temperature of 126 °C begin to

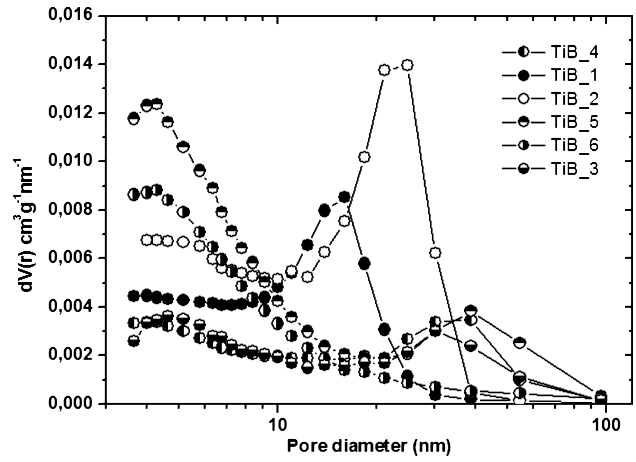

FIGURE 3. BHJ pore size distribution using desorption curve d$V(r)$ versus pore radius of prepared boron-doped titania.

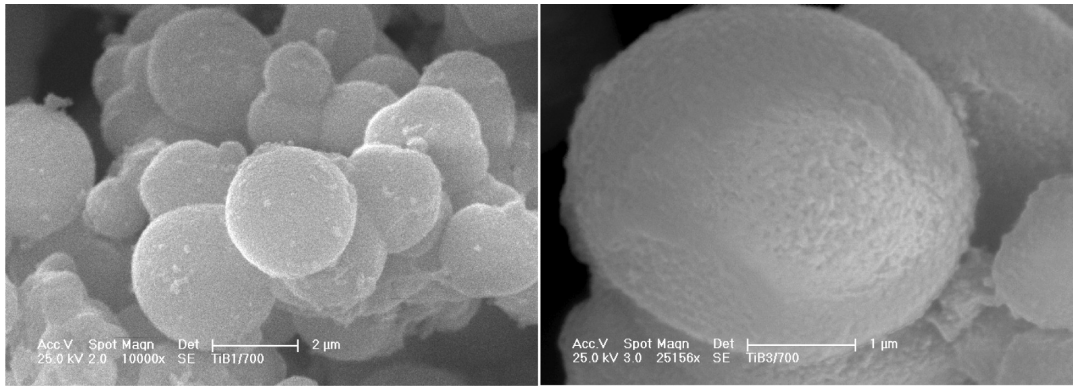

FIGURE 4. SEM images of the sample TiB1_700 (on the left) and TiB3_700 (on the right).

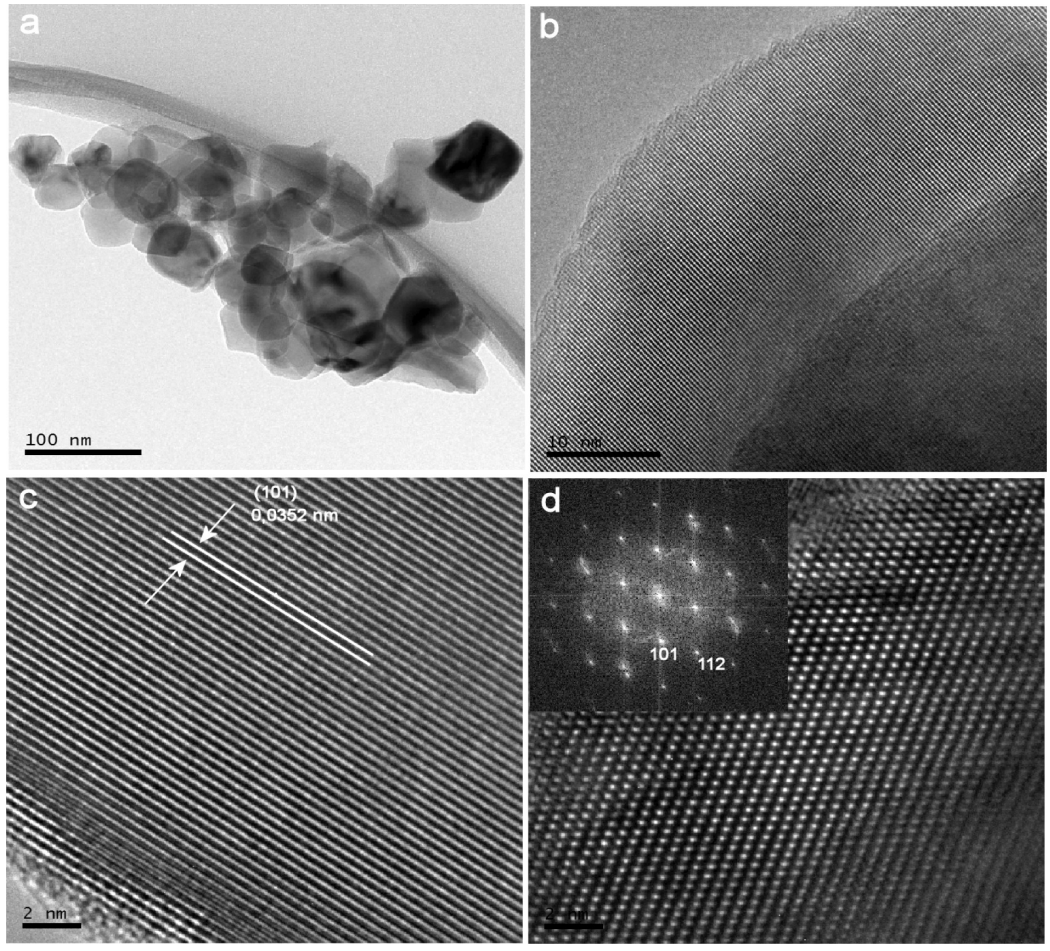

FIGURE 5. HRTEM micrograph of the sample TiB_3 annealed at 700 °C: (a) magnification 40 000×, (b) magnification 400 000×, (c, d) magnification 1 000 000×; inset is FFTs.

evolve water and impurity of adsorbed carbonates. Next exothermic peak begins at temperature of 697 °C (maximum at 766 °C) and corresponds to oxidation of amorphous boron.

3.3. Surface Area and Porosity (BET and BJH). The specific surface area (S_{BET}) calculated from the BET method (18) is shown in Table 1. The results show that specific surface areas of titania samples have tendency to decrease with increasing content of boron. The pore size distribution curves (d$V(r)$ vs pore radius) of the prepared samples (see Figure 3) indicate conversion from micropores to mesopores with increasing amount of boron, but samples with the highest content of B (sample TiB_5, TiB_6) become microporous again, which is probably caused by the presence of sassolite (H_3BO_3) in these samples. The maximum pore volume was reached by sample TiB_3.

3.4. Scanning Electron Microscopy (SEM) and High-Resolution Transmission Electron Microscopy (HRTEM). Figure 4 shows SEM micrograph of boron doped titania (samples TiB_3) heated at 700 °C. As we reported earlier (23), the homogeneous hydrolysis of $TiOSO_4$ with urea leads to anatase nanoparticles assembled into

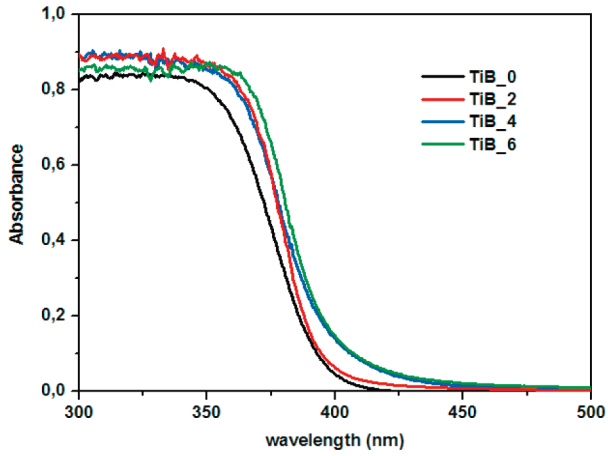

FIGURE 6. Absorbance UV/vis spectra of prepared B-doped titania and undoped titania (TiB_0); samples annealed at 700 °C.

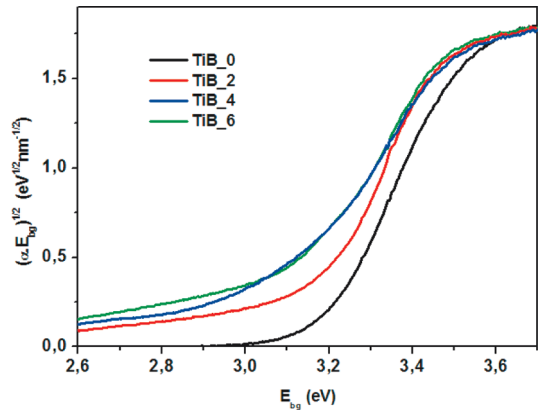

FIGURE 7. Band-gap energy of B-doped samples and undoped titania (TiB_0); samples annealed at 700 °C.

spherical clusters of diameter ca. 1−2 μm. It was observed that titania samples doped with boron form spherical agglomerates with the average size ca. 1−3 μm. Figure 5 shows micrographs of TiB_3 sample obtained by high-resolution transmission microscopy (HRTEM). These images showed no evidence of extended planar distance. The fine fringe spacing is 0.35 nm and corresponds to (101) plane of anatase.

3.5. UV/Vis Spectra and Band Gap Energy. UV−vis absorption spectra of the prepared boron doped titania samples are showed in Figure 6. The intensity of the absorbance in the visible region increases with the concentration of the B ion. The spectra show red-shift in the band gap transition and the absorption edge shift to longer wavelength is caused by boron content. With regard to the results from XRD analysis, it could be concluded that boron doping led to the coprecipitation of two of the titania polymorphs, rutile and anatase, and implicate the decreasing band gap energies and visible-light activation (7).

The method of UV/vis diffuse reflectance spectroscopy was employed to estimate band gap energies of the boron doped titania samples. First, to establish the type of band-to-band transition in the synthesized particles, the absorption data were fitted to equations for direct band gap transitions. The minimum wavelength required to promote an electron depends upon the band gap energy E_{bg} of the photocatalyst and is given by eq 1:

$$E_{bg} = 1240/\lambda \text{ (eV)}, \quad (1)$$

where λ is the wavelength in nanometers (24, 25).

Figure 7 shows the $(\alpha E_{bg})^2$ versus E_{bg} for a indirect band gap transition of boron doped titania where α is the absorption coefficient and E_{bg} is the photon energy. The value of E_{bg} extrapolated to $\alpha = 0$ gives an absorption energy that corresponds to a band-gap energy (see Table 2). The value of 3.20 eV, for sample, denoted as TiB_0 is reported in the literature for pure TiO_2 anatase nanoparticles (24). Band-gap energy of the doped samples decreases with increasing

Table 2. Band-Gap Energy of Samples and Rate Constants *k* of Orange IIPhotodegradation by Prepared Samples

		k (min^{-1})		
sample	band gap (eV)	365 nm	400 nm (bio light)	400 nm (warm white)
TiB0_700	3.2	0.0397	0.0033	0.0025
TiB1_700	3.15	0.0262	0.0073	0.0067
TiB2_700	3.1	0.0244	0.0064	0.0056
TiB3_700	3.1	0.0362	0.0106	0.0124
TiB4_700	3.0	0.0170	0.0036	0.0048
TiB5_700	3.0	0.0355	0.0068	0.0090
TiB6_700	3.0	0.0174	0.0035	0.0051

content of boron ions. The color density of prepared samples depends on the amount of boron dopant and its hue is yellowish.

3.6. Photocatalytic Activity. The photocatalytic activity of titania doped with boron ions was determined by degradation of Orange II aqueous solutions under UV radiation (at 365 nm). In regions where Lambert−Beer law (eq 2) is significant, the concentration of Orange II dye is proportional to absorbance.

$$A = \varepsilon cl \quad (2)$$

where A is absorbance, c is concentration of absorbing component, l is length of absorbing layer, and ε is the molar absorbing coefficient. The time dependences of Orange II dye decomposition can be described by using eq 3 for the first kinetics reaction (26)

$$\frac{d[\text{OII}]}{dt} = k(a_0 - [\text{OII}]) \quad (3)$$

where [OII] is concentration of Orange II dye, a_0 is initial concentration of Orange II dye, and k is rate constant. For comparison, the photocatalytic activity of undoped anatase TiO_2 was also tested (sample TiB0_700). The calculated degradation rate constants k (min^{-1}) are shown in Table 2 and example kinetics of degradation of Orange II

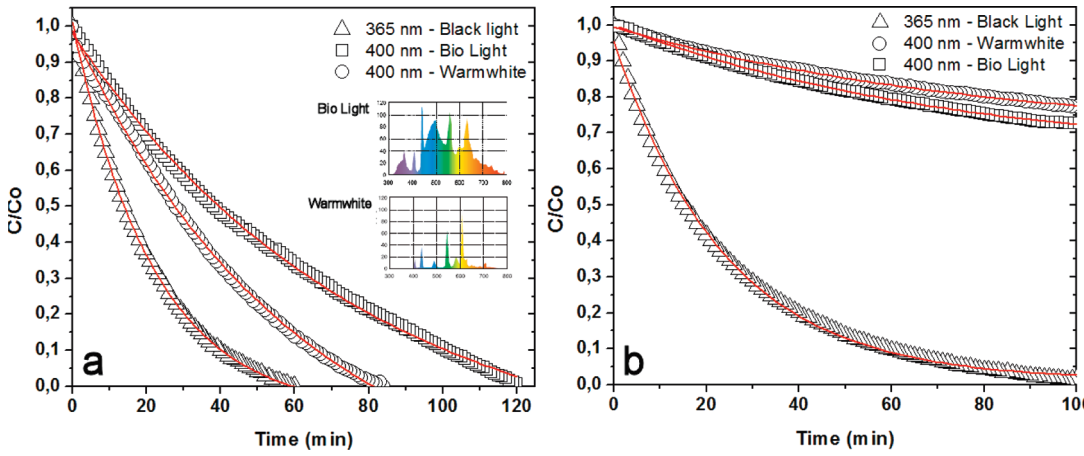

FIGURE 8. Photocatalytic activity of (a) sample TiB3_700, (b) undoped titania TiB0_700.

dye at 365 nm (black light) and 400 nm (Bio light and Warmwhite) on sample TiB3_700 and TiB0_700 are illustrated in Figure 8. As indicated in Table 2, undoped anatase (sample TiB0_700) exhibits very low visible-light photocatalytic activity for degradation of Orange II dye. This is caused by the higher band gap energy of anatase (3.2 eV, $\lambda_{bg} = 388$ nm) and rutile (3.0 eV, $\lambda_{bg} = 413$ nm) (27). The photocatalysts prepared by homogeneous hydrolysis of $TiOSO_4$ in the presence of boron, namely sample TiB3_700, exhibited the higher photoactivity under visible light in comparison with the undoped TiO_2. The addition of a higher amount of boron dopant (i.e., 0.75% and more) results in appearance of sassolite phase, H_3BO_3, and causes the loss in photocatalytic activity. Samples with higher content of boron (TiB_4, TiB_5, and TiB_6) annealed at 700 °C consists not only of anatase but also of rutile modification. These results indicate that the content of rutile phase increases with the increase amount of amorphous boron. Also, the results showed that doping with boron in range from 0.75 to 3.0 g means band gap decreasing to 3.0 eV (see Table 2). The occurrence of a higher amount of rutile and sassolite H_3BO_3 phase inhibits significantly the photocatalytic activity.

4. CONCLUSIONS

Nanosized boron-doped titania was prepared by homogeneous hydrolysis of titanium oxo-sulfate with urea in aqueous solutions in the presence of amorphous boron. The prepared samples were annealed at 700 °C. The highest photoactivity under visible light was observed for sample TiB3_700 prepared by homogeneous hydrolysis with 0.5 g of amorphous boron. Well-crystallized small TiO_2 particles (less than 100 nm) with anatase crystal structure and boron occupied the interstitials between the TiO_2 crystallites have a great role for improvement of microstructure properties such as high surface area and pore volume that result in better photocatalytic activity. However, a higher content of boron dopant and annealing at 700 °C causes the occurrence of sassolite and rutile phases, which result in decreasing photocatalytic properties.

Acknowledgment. The work was supported by the Academy of Sciences of the Czech Republic (Project AV0Z40320502) and Czech Science Foundation (Project 203/08/0335).

REFERENCES AND NOTES

(1) Ling, Q.; Sun, J.; Zhou, Q. *Appl. Surf. Sci.* **2008**, *254*, 3236–3241.
(2) Khan, R.; Kim, S.; Kim, T.; Nam, C. *Mater. Chem. Phys.* **2008**, *112*, 167–172.
(3) Ling, Q.; Sun, J.; Zhou, Q.; Zhao, Q.; Ren, H. *J. Photochem. Photobiol., A: Chem.* **2008**, *200*, 141–147.
(4) Zhang, X.; Liu, Q. *Mater. Lett.* **2008**, *62*, 2589–2592.
(5) Gombac, V.; De Rogatis, L.; Gasparotto, A.; Vicario, G.; Montini, T.; Barreca, D.; Balducci, G.; Fornasiero, P.; Tondello, E.; Graziani, M. *Chem. Phys.* **2007**, *339*, 111–123.
(6) Ma, Z.; Zhang, L.; Chen, R.; Xing, W.; Xu, N. *Chem. Eng. J.* **2008**, *138*, 517–522.
(7) Zaleska, A.; Sobczak, J. W.; Grabowska, E.; Hupka, J. *Appl. Catal. B: Environ.* **2008**, *78*, 92–100.
(8) Wei, C.; Tang, X.; Liang, J.; Tan, S. *J. Environ. Sci.* **2007**, *19*, 90–96.
(9) Su, Y.; Han, S.; Zhang, X.; Chen, X.; Lei, L. *Mater. Chem. Phys.* **2008**, *110*, 239–246.
(10) Lu, N.; Zhao, H.; Li, J.; Quan, X.; Chen, S. *Separ. Purif. Technol.* **2008**, *62*, 668–673.
(11) Ling, Q.; Sun, J.; Zhou, Q.; Ren, H.; Zhao, Q. *Appl. Surf. Sci.* **2008**, *254*, 6731–6735.
(12) Zaleska, A.; Grabowska, E.; Sobczak, J. W.; Gazda, M.; Hupka, J. *Appl. Catal., B* **2009**, *89*, 469–475.
(13) Moon, S.; Mametsuka, H.; Tabata, S.; Suzuki, E. *Catal. Today* **2000**, *58*, 125–132.
(14) Chen, D.; Yang, D.; Wang, Q.; Jiang, Z. *Ind. Eng. Chem. Res.* **2006**, *45*, 4110–4116.
(15) Bettinelli, M.; Dallacasa, V.; Falcomer, D.; Fornasiero, P.; Gombac, V.; Montini, T.; Romano, L.; Speghini, A. *J. Hazard. Mater.* **2007**, *146*, 529–534.
(16) *JCPDS PDF-2 release 2001*, International Center for Diffraction Data: Newtown Square, PA, 2001.
(17) *ICSD Database*; FIZ Karlsruhe: Karlsruhe, Germany, 2008.
(18) Brunauer, S.; Emmett, P. H.; Teller, E. *J. Am. Chem. Soc.* **1938**, *60*, 309–319.
(19) Barret, E. P.; Joyner, L. G.; Halenda, P. P. *J. Am. Chem. Soc.* **1951**, *73*, 373–380.
(20) Orel, Z. C.; Gunde, M. K.; Orel, B. *Prog. Org. Coat.* **1997**, *30*, 59–66.
(21) Štengl, V.; Houšková, V.; Bakardjieva, S.; Murafa, N.; Havlín, V. *J. Phys. Chem. C* **2008**, *112*, 19979–19985.
(22) Monteagudo, J. M.; Durán, A. *Chemosphere* **2006**, *65*, 1242–1248.
(23) Bakardjieva, S.; Šubrt, J.; Štengl, V.; Dianez, M. J.; Sayagues, M. J. *Appl. Catal., B* **2005**, *58*, 193–202.
(24) Bhatkhande, D. S.; Pangarkar, V. G.; Beenackers, A. A. *J. Chem. Technol. Biotechnol.* **2001**, *77*, 102–116.
(25) Reddy, K. M.; Panorama, S. V.; Reddy, A. R. *Mater. Chem. Phys.* **2002**, *78*, 239–245.
(26) Macounová, M.; Krýsová, H.; Ludvík, J.; Jirkovský, J. *J. Photochem. Photobiol., A: Chem.* **2003**, *156*, 273–282.
(27) Nagaveni, K.; Sivalingan, G.; Hegde, M. S.; Madras, G. *Appl. Catal., B* **2004**, *48*, 83–93.

AM9007598